OPEN ACCESS



Synthesis and Spectroscopic Characterization of Interstellar Candidate Ethynyl Thiocyanate: HCCSCN

Elena R. Alonso¹, Aran Insausti², Lucie Kolesniková³, Iker León¹, Brett A. McGuire^{4,5}, Christopher N. Shingledecker⁶, Marcelino Agúndez⁷, José Cernicharo⁷, Víctor M. Rivilla⁸, Carlos Cabezas⁷, Izaskun Jiménez-Serra⁸, Jesús Martín-Pintado⁸, and Jean-Claude Guillemin⁹, Carlos Cabezas⁷, and Jean-Claude Guillemin⁹, Grupo de Espectroscopía Molecular (GEM), Edificio Quifima, Laboratorios de Espectroscopía y Bioespectroscopia, Universidad de Valladolid, Aroll Valladolid, Spain; elenarita.alonso@uva.es

Departamento de Química Física, Facultad de Ciencia y Tecnología, Universidad del País Vasco (UPV/EHU), 48940 Leioa, Spain Department of Analytical Chemistry, University of Chemistry and Technology, Technická 5, 16628 Prague 6, Czech Republic

⁴ Department of Chemistry, Massachusetts Institute of Technology, Cambridge, MA 02139, USA

⁵ National Radio Astronomy Observatory, Charlottesville, VA 22903, USA

⁶ Department of Chemistry, Virginia Military Institute, Lexington, VA 24450, USA

⁷ Instituto de Física Fundamental, CSIC, Calle Serrano 123, 28006 Madrid, Spain

⁸ Centro de Astrobiología (CSIC-INTA), Ctra. de Ajalvir Km. 4, Torrejón de Ardoz, 28850 Madrid, Spain

⁹ Univ Rennes, Ecole Nationale Supérieure de Chimie de Rennes, CNRS, ISCR- UMR 6226, Rennes, France Received 2024 July 1; revised 2024 October 4; accepted 2024 October 6; published 2024 November 14

Abstract

This work aims to spectroscopically characterize and provide for the first time direct experimental frequencies of the ground vibrational state and two excited states of the simplest alkynyl thiocyanate (HCCSCN) for astrophysical use. Both microwave (8–16 GHz) and millimeter-wave regions (50–120 GHz) of the spectrum have been measured and analyzed in terms of Watson's semirigid rotor Hamiltonian. A total of 314 transitions were assigned to the ground state of HCCSCN, and a first set of spectroscopic constants have been accurately determined. Spectral features of the molecule were then searched for in Sgr B2(N), NGC 6334I, G+0.693–0.027, and TMC-1 molecular clouds. Upper limits to the column density are provided.

Unified Astronomy Thesaurus concepts: Microwave spectroscopy (2251); Millimeter-wave spectroscopy (2252); Molecular spectroscopy (2095); Rotational spectroscopy (2248); Interstellar medium (847); Radio astronomy (1338)

Materials only available in the online version of record: machine-readable table

1. Introduction

In the last years, there has been a renewed interest on the chemistry of sulfur in the interstellar medium (ISM), aiming to shed light on the long-standing problem of the missing sulfur. That is, in cold dense clouds, all detected S-bearing molecules only account for a very small fraction of sulfur, meaning that the main reservoir of sulfur is unknown (T. H. G. Vidal et al. 2017). Motivated by this interest, a large variety of sulfurbearing molecules have been detected in the ISM on the basis of their pure rotational spectrum. Recent detections of S-bearing molecules include S₂H (A. Fuente et al. 2017), NS⁺ (J. Cernicharo et al. 2018), HCS, HSC (M. Agúndez et al. 2018), HC₃S⁺ (J. Cernicharo et al. 2021d), NCS, HCCS, H₂CCS, H₂CCCS, C₄S, C₅S (J. Cernicharo et al. 2021b), HC(O)SH, C₂H₅SH (L. F. Rodríguez-Almeida et al. 2021a), HCSCN, HCSCCH (J. Cernicharo et al. 2021c), HCCS⁺ (C. Cabezas et al. 2022), HC₄S (R. Fuentetaja et al. 2022), HSO (N. Marcelino et al. 2023), HCNS (J. Cernicharo et al. 2024), HOCS⁺ (M. Sanz-Novo et al. 2024a), and HNSO (M. Sanz-Novo et al. 2024b). Although the problem of the missing sulfur remains open, this plethora of detections has shown that sulfur participates in a particularly rich chemistry.

Original content from this work may be used under the terms of the Creative Commons Attribution 4.0 licence. Any further distribution of this work must maintain attribution to the author(s) and the title of the work, journal citation and DOI.

A particularly interesting case of S-bearing molecules is the CHNS family, in which three different isomers have been detected in the ISM. The three detected isomers, in increasing energy, are thioisocyanic acid (HNCS; M. A. Frerking et al. 1979), thiocyanic acid (HSCN; S. Brünken et al. 2009; D. T. Halfen et al. 2009; G. R. Adande et al. 2010), and thiofulminic acid (HCNS; B. A. McGuire et al. 2016; J. Cernicharo et al. 2024). The most stable isomer is HNCS, while HSCN and HCNS lie 3200 and 17,300 K above, respectively (M. Wierzejewska & J. Moc 2003; B. A. McGuire et al. 2016). In spite of this ordering in energy, it turns out that in the cold starless core TMC-1, the most abundant isomer is HSCN, which is not the most stable one (J. Cernicharo et al. 2024). Given that these molecules are relatively abundant in interstellar clouds such as Sgr B2N, NGC 63341, G+0.693 -0.027, and TMC-1, derivatives in which a CN or CCH group substitutes one hydrogen atom are good targets for astronomical detection. Taking into account the observed abundance of HSCN, it seems promising to search for the CN and CCH derivatives of HSCN, in particular HCCSCN, which is an isomer of the recently detected NCCHCS species in TMC-1 (C. Cabezas et al. 2024).

In this paper, we present the first measurements of the pure rotational spectrum of ethynyl thiocyanate (HCCSCN), the CCH derivative of HSCN (see Figure 1), and an astronomical search for it toward several molecular clouds. The molecule has been first synthesized by B. Lu et al. (2021) and only characterized by UV-Vis and IR spectroscopy. HCCSCN is

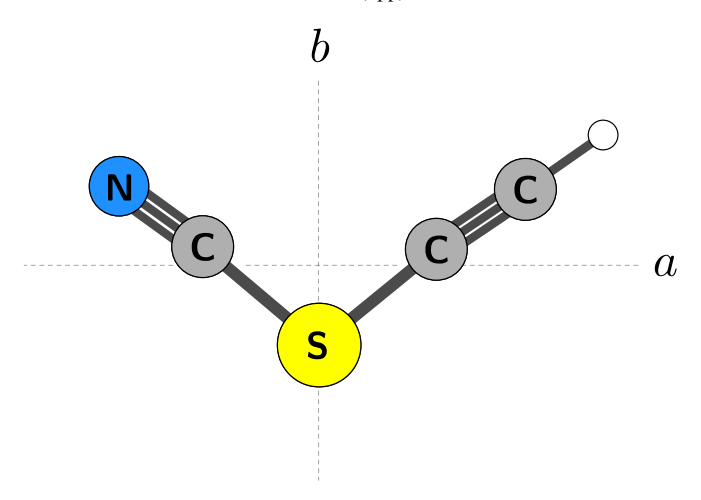


Figure 1. Optimized structure of the HCCSCN molecule depicted in the $\it ab$ inertial plane.

predicted as the third most stable acyclic structure in the HC₃NS family of isomers, right after NCC(H)CS and HCCNCS (B. Lu et al. 2021).

2. Experimental Methodology

Searching for and detecting a new molecule in the ISM typically begins on Earth at a spectroscopic laboratory. This work has been carried out in synergy between an organic chemist, spectroscopists, and astrophysicists. This work tandem has been very successful in the detection of more than 310 molecules in the ISM or circumstellar shells up to the present day (C. P. Endres et al. 2016). The followed working procedure to obtain a set of parameters that the astrophysicist uses to carry out the complex search for molecules in the different regions of the ISM includes, in many cases, complex chemical synthesis, the use of home-built and expensive experimental techniques, as well as computational methodology for the calculation of molecular structures.

2.1. Chemical Synthesis

The ethynyl thiocyanate has been synthesized by reacting alkynyl(phenyl)iodonium trifluoromethanesulfonate with sodium thiocyanate (B. Lu et al. 2021). In this work, it has been prepared by reacting tributylethynylstannane with sulfur cyanide, with a yield of 63%. A similar approach has been used in the past to synthesize 1,2-propadien-1-ylthiocyanate. The compound, which is kinetically unstable, was stabilized in a high-boiling solvent (diethyleneglycol dibutyl ether) in the presence of small amounts of duroquinone (a high-boiling radical inhibitor) and conserved in dry ice.

2.2. Rotational Spectra

In the first step, the broadband rotational spectrum of HCCSCN was recorded from 8 to 21 GHz employing the Chirped-Pulse Fourier Transform Microwave (CP-FTMW) spectrometer of the Universidad de Valladolid (C. Cabezas et al. 2017; I. León et al. 2019). The synthesized liquid sample, highly volatile, was deposited in a small sealed container through which a carrier gas, Neon, was passed at a pressure of 10–12 bar. This container was introduced in a cooling bath with dry ice to minimize the quick decomposition of the sample. The molecules seeded in the carrier gas were adiabatically expanded

through a nozzle (1 mm in diameter) and probed in the cold and efficiently isolated conditions of a supersonic expansion. Then, sequentially, the molecules were polarized using a high power excitation pulse of 300 W to then capture up to 60,000 free induction decays that were averaged in the time domain and Fourier transformed to obtain the spectrum in the frequency domain. Figure 2 shows the obtained CP-FTMW spectrum.

After completing the broadband microwave range experiment, we moved on to the millimeter-wave range, recording the room-temperature rotational spectrum using the Valladolid home-built millimeter-wave absorption spectrometer (A. M. Daly et al. 2014; L. Kolesniková et al. 2017). Employing a multiplication (4× and 6×; VDI, Inc.) of the basic synthesizer frequency (Agilent; 250 kHz–20 GHz), the frequency range from 50 to 120 GHz was reached. The synthesizer output was frequency modulated at 10.2 kHz with a modulation depth between 50 and 60 kHz. A Schottky diode detector (VDI, Inc.) was used to capture the signal after a double radiation pass through the cell, and then it was introduced in a lock-in amplifier. A second derivative shape of the lines resulting from 2f detection was fitted to the Gaussian profile function. The uncertainty of the line center frequency is estimated to be better than 50 kHz.

2.3. Quantum Chemical Calculations

To be able to interpret the rotational spectra, it is very useful to have theoretically predicted rotational parameters. For this, it is necessary to have an optimized geometry of the molecule, which can be obtained using computational calculations. Since HCCSCN has only six atoms, a triple bond between the carbons and a thiocyanate group, it can form only a single conformation, thereby simplifying the computational process.

The geometry optimization was done employing both density functional theory (DFT) and *ab initio* computational methods implemented in Gaussian 16 (M. J. Frisch et al. 2016). The levels of theory used were the B3LYP density functional (A. D. Becke 1992, 1993), including the Grimme D3 dispersion interactions (S. Grimme et al. 2010) with Becke–Johnson damping (S. Grimme et al. 2011), and the Møller–Plesset second-order method (C. Møller & M. S. Plesset 1934), respectively. The basis set employed in both cases is the Pople split-valence triple-zeta basis set augmented with diffuse and polarization functions on all atoms (the 6-311++G (d,p) basis set; M. J. Frisch et al. 1984).

Furthermore, the frequencies of the vibrational modes were also calculated at the same B3LYP density functional and the same basis set employed in the geometry optimization mentioned above. The calculation of the first-order vibration-rotation correction constants α_i , which define the well-known vibrational dependence of rotational constants, was used to derive the changes in rotational constants according to the following equation: $B_v = B_e - \sum_i \alpha_i (v_i + 1/2)$, where B_v and B_e substitute all three rotational constants in a given vibrational state and in equilibrium, respectively, and v_i is the vibrational quantum number of the ith vibrational mode. This allowed to assign the two excited states found in our spectra based on the differences between theoretical and experimental rotational constants.

3. Analysis of the Spectra

The observation of characteristic transition patterns is extremely helpful in searches and assignments of the spectrum of a new species, and if possible, it is useful to start at the

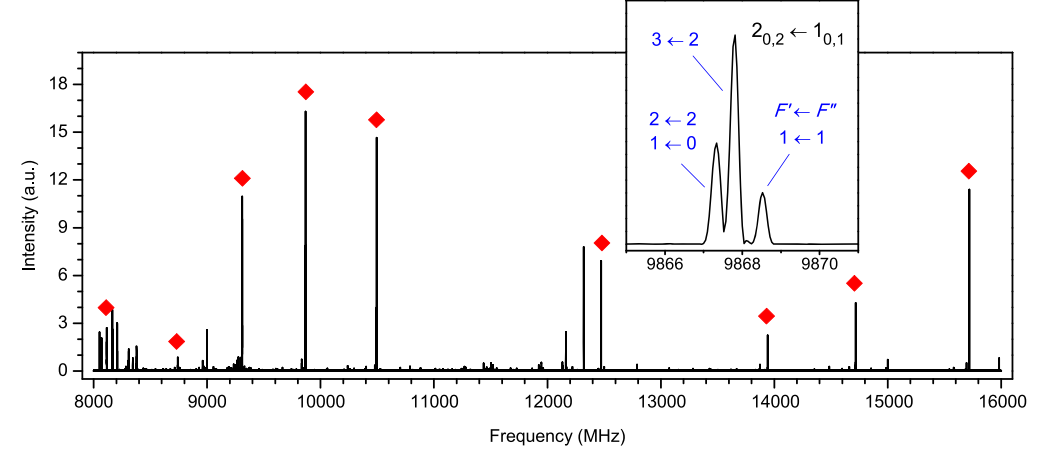


Figure 2. Broadband CP-FTMW spectrum of HCCSCN. The red rhombus indicates measured transition. The inset shows the nuclear quadrupole hyperfine structure for $2_{0.2} \leftarrow 1_{0.1}$ rotational transition.

lower-frequency range. We therefore first relied on our broadband spectra measurements carried out with the CP-FTMW spectrometer. HCCSCN is a prolate asymmetric rotor and is predicted to have dipole moment components along the a and b inertial axes ($|\mu_a| = 3.2 \,\mathrm{D}$, $|\mu_b| = 1.2 \,\mathrm{D}$).

The recorded broadband spectrum indeed presented very intense lines. The assignment of these intense lines was straightforward to the a-type R-branch typical triad of transitions: $2_{0,2} \leftarrow 1_{0,1}$; $2_{1,1} \leftarrow 1_{1,0}$; $2_{1,2} \leftarrow 1_{1,1}$ and $3_{0,3} \leftarrow 2_{0,2}$; $3_{1,3} \leftarrow 2_{1,2}$; $3_{1,2} \leftarrow 2_{1,1}$. Then *b*-type R-branch transitions were also measured. We could observe that all these transitions present a hyperfine structure (see Figure 2) due to the presence of ^{14}N in the molecule, with nuclear spin (I=1) and nonzero electric quadrupole moment, which interacts with the electric field gradient of the molecule at the position of this nucleus and causes the splitting of each rotational level into several sublevels (W. Gordy & R. L. Cook 1984). A total of 13 transitions with 43 hyperfine components were measured with an assumed frequency accuracy of 10 kHz. A first set of rotational constants was obtained using a Watson's A-reduced semirigid rotor analysis in the I^r-representation, adding a term to account for the nuclear quadrupole coupling contribution (H. M. Foley 1947; G. W. Robinson & C. D. Cornwell 1953), enabling the determination of the ¹⁴N nuclear quadrupole coupling constants. Some lines in the spectrum remain unassigned and could be attributed to transitions of some compounds from the synthesis or some perturbed and unassigned excited vibrational states. The most prominent spectral features are accounted in our analyses and follow the expected spectral pattern of HCCSCN.

With this first set of rotational parameters a prediction of the transitions at higher frequencies was done, and we proceeded to the analysis of the millimeter-wave spectrum in the 50–120 GHz frequency range. The prediction presented a shift in the frequency of the transitions with respect to the experimental ones due to the centrifugal distortion effects, but it was not difficult to find the transition patterns that led to measure a total of 271 additional transitions of the molecule with an assumed frequency accuracy of 30 kHz. In this frequency range, the hyperfine structure collapses into a single line, simplifying the spectra. The final fit, combining the transitions from both microwave and millimeter-wave experiments with their corresponding weights, was obtained using Watson's A-reduced Hamiltonian in the I'-representation

(J. K. G. Watson 1977) and Pickett's SPFIT/SPCAT program suite (H. M. Pickett 1991). (All measured transitions are available in a machine-readable form in the online journal.) The spectroscopic data obtained in this work allowed the determination of the rotational constants, nuclear quadrupole coupling constants, as well as the full set of quartic and some sextic centrifugal distortion constants presented in Table 1. This spectroscopic information thus enables a search for this newly characterized molecule in different regions of the ISM.

Further inspection of the spectrum revealed the existence of satellite lines in the neighborhood of the ground state. These lines most likely belong to pure rotational transitions in excited vibrational states. Under the C_s point group, the lowest-frequency normal vibrational mode is ν_9 (A'), with the anharmonic frequency predicted at 118 cm⁻¹. This vibrational mode corresponds to scissoring bending vibration. As Figure 3 shows, we were able to follow two successive excitations of this mode and to assign over 160 and 40 lines for $\nu_9 = 1$ and $\nu_9 = 2$ excited vibrational states, respectively. The assignment was carried out by comparing the values of their experimental changes in rotational constants relative to the ground state with their calculated counterparts; see Table 2. Only a-type transitions have been observed for both excited vibrational states. (All measured transitions are available in a machine-readable form in the online journal.)

4. Observational Searches

Sgr B2N. We have searched for signal from HCCSCN in the Prebiotic Interstellar Molecular Survey (PRIMOS) project observations toward Sgr B2(N) using the 100 m Robert C Byrd Green Bank Telescope (GBT). Sgr B2(N) is a massive star-forming region (B. E. Turner 1991) located at a distance of \sim 8.3 kpc (M. J. Reid et al. 2014). The details of this data set are presented elsewhere (J. L. Neill et al. 2012), and only a few pertinent details will be summarized. The observations were taken in position-switched mode, with the pointing position set to (J2000) $\alpha = 17^{\rm h}47^{\rm m}19.^{\rm s}8$, $\delta = -28^{\circ}22^{\prime}17^{\prime\prime}$. The bandwidth covers a total range of 1–50 GHz with a few gaps, primarily at the lower frequencies, and at a resolution of \sim 24 kHz corresponding to 2–0.14 km s⁻¹ across the band. The rms sensitivity ranges from a few to a few tens of mK.

Molecules in Sgr B2(N) observations typically fall into one of two categories: cold, extended, and in absorption (e.g.,

Table 1
Spectroscopic Constants of HCCSCN in the Ground State (G.S.) and Two Excited Vibrational States (A-Reduction, I'-Representation) in Comparison with Quantum Chemical Calculations

Parameter	G.S. ^a	$v_9 = 1^a$	$v_9 = 2^a$	Calculated ^b
A/MHz	10294.7535(31)	10390.088(34)	10486.759(48)	10458
B/MHz	2771.73159(44)	2782.19440(92)	2792.5389(18)	2717
C/MHz	2179.00087(41)	2180.95866(55)	2182.85772(97)	2156
Δ_J/kHz	1.95771(80)	1.97331(69)	1.9898(13)	1.78
Δ_{JK}/kHz	-32.1930(30)	-32.4694(59)	-32.759(11)	-31.02
$\Delta_{\it K}/{ m kHz}$	195.19(63)	201.7(13)	211.1(19)	199.07
δ_J/kHz	0.76512(25)	0.77350(38)	0.78425(75)	0.68
δ_K/kHz	2.843(21)	3.570(30)	4.365(47)	2.39
$\Phi_J/{ m mHz}$	9.11(78)	9.11 ^c	9.11 ^c	8.64
Φ_{JK}/mHz	-87.5(37)	-95.6(61)	-87.5^{c}	-64.39
Φ_{KJ}/Hz	-1.1064(59)	-1.1064^{c}	-1.1064^{c}	-1.21
Φ_K/Hz	[11.85] ^d	[11.85] ^d	[11.85] ^d	11.85
ϕ_J/mHz	[4.14] ^d	[4.14] ^d	[4.14] ^d	4.14
ϕ_{JK}/mHz	[5.47] ^d	[5.47] ^d	[5.47] ^d	5.47
ϕ_K/Hz	[1.36] ^d	[1.36] ^d	[1.36] ^d	1.36
$\chi_{aa}/{ m MHz}$	-1.5260(73)		•••	-1.69
$\chi_{bb}/{ m MHz}$	0.290(10)		•••	0.49
$\chi_{cc}/{ m MHz}$	1.236(10)		•••	1.20
$J_{ m min}/J_{ m max}$	1/25	9/26	11/24	
K_a^{\min}/K_a^{\max}	0/20	0/15	0/7	
N ^e	314	165	43	•••
$\sigma_{\rm fit}^{}/{ m MHz}$	0.020	0.043	0.028	
$\sigma_{ m w}^{\ \ g}$	0.88	0.87	0.94	

Notes

(This table is available in its entirety in machine-readable form in the online article.)

B. A. McGuire et al. 2016) or warm, compact, and in emission (e.g., A. Belloche et al. 2013). We therefore searched for HCCSCN under two sets of conditions using a singleexcitation model: a cold model with $T_{\rm ex} = 5.8$ K with a 20" source size and a warm model with $T_{\rm ex}=150\,{\rm K}$ with a 5" source size. The line width was $8\,{\rm km\,s}^{-1}$ and the $V_{\rm LSR}$ was +64 km s⁻¹ in both cases. At any reasonable line width, splitting due to hyperfine components is negligible and unresolved. The 3σ upper limit was set using what would be the highest signal-to-noise ratio line in the case of a detection. No signal was seen consistent with either scenario, and explorations of the data preclude any detection at other excitation temperatures as well. The 3σ upper limit for warm HCCSCN was $N_T \le 5 \times 10^{15} \, \mathrm{cm}^{-2}$ and for cold HCCSCN was $N_T \le 8 \times 10^{12} \, \mathrm{cm}^{-2}$. This corresponds to a fractional abundance of $X_{\mathrm{H_2}} \le 8 \times 10^{-12} \, \mathrm{cm}^{-2}$ assuming an $N_{\mathrm{H_2}} = 1 \times 10^{-12} \, \mathrm{cm}^{-2}$ $10^{24}\,\mathrm{cm}^{-2}$ (D. C. Lis & P. F. Goldsmith 1990). The much more stringent limit in the case of cold HCCSCN is due to the substantially reduced partition function, which would result in far stronger transitions (relatively speaking) at these frequencies. The rotational partition function (Q_{rot}) was evaluated by summation of the Boltzmann factors over the energy levels in

the ground vibrational state; see Table 3. We used the SPCAT program (H. M. Pickett et al. 1998) to undertake this summation, numerically employing the spectroscopic constants from Table 1 and all rotational states up to J = 250 and $K_a = 150$. Figure 4 shows the constraining transitions in each case.

NGC 6334I. We have also searched for signal in Atacama Large Millimeter/sub-Millimeter Array (ALMA) observations of the massive star-forming region NGC 6334I. The data set used here is the same that was used for the first interstellar detection of methoxymethanol (CH₃OCH₂OH; B. A. McGuire et al. 2017). The most constraining transition is located near ~280.8 GHz in data from Project #2015.A.00022.T. The phase center for the observations was (J2000) $\alpha =$ $17^{h}20^{m}53^{s}.36$, $\delta = -35^{\circ}47'00''.0$. The angular resolution achieved was 0.25×0.19 , with a spectral resolution of $1.1 \,\mathrm{km \, s^{-1}}$ and a sensitivity of $2.0 \,\mathrm{mJy \, beam^{-1}}$. The extraction position for the spectra that were investigated was (J2000) $\alpha = 17^{\rm h}20^{\rm m}53.^{\rm s}373, \ \delta = -35^{\circ}46'58.''14$, the same position in which CH3OCH2OH was originally detected. We use the same excitation temperature ($T_{\rm ex} = 200 \, \rm K$), line width ($\Delta V = 2.4 \, \rm km \, s^{-1}$), and $V_{\rm lsr} = -7 \, \rm km \, s^{-1}$ as in that work and assume the source fills the beam. As with Sgr B2(N), hyperfine splitting is unresolved. We derive an upper limit of

^a The numbers in parentheses for all the experimentally determined parameters are their uncertainties in units of the last decimal digits. Their values are close to 1σ standard uncertainties because the unitless (weighted) deviation of the fit is close to 1.0. The SPFIT/SPCAT program package (H. M. Pickett 1991) was used for the analysis

^b Equilibrium values calculated at B3LYP/6-311++G(d,p) level of theory.

^c Values fixed to the ones fitted for G.S.

^d Values in brackets fixed to those calculated theoretically.

e Number of distinct frequency lines in the fit. All measured transitions are available in a machine-readable form in the online journal.

f Rms deviation of the fit.

^g Unitless (weighted) deviation of the fit.

Table 2 Vibrational Changes in Rotational Constants for the $v_9 = 1$ and $v_9 = 2$ Excited Vibrational States

	$v_9 = 1$		$v_9 = 2$	
	Exp.	Calculated ^a	Exp.	Estimated ^b
$A_v - A_0 / \text{MHz}$	-95.334(34)	-102.21	-192.005(48)	-190.67
$B_v - B_0 / \text{MHz}$	-10.4628(10)	-9.36	-20.8073(19)	-20.93
$C_v - C_0/\mathrm{MHz}$	-1.95779(68)	-1.75	-3.8569(11)	-3.92

Notes.

^b Estimated from experimental changes listed for $v_9 = 1$ by assuming their additivity.

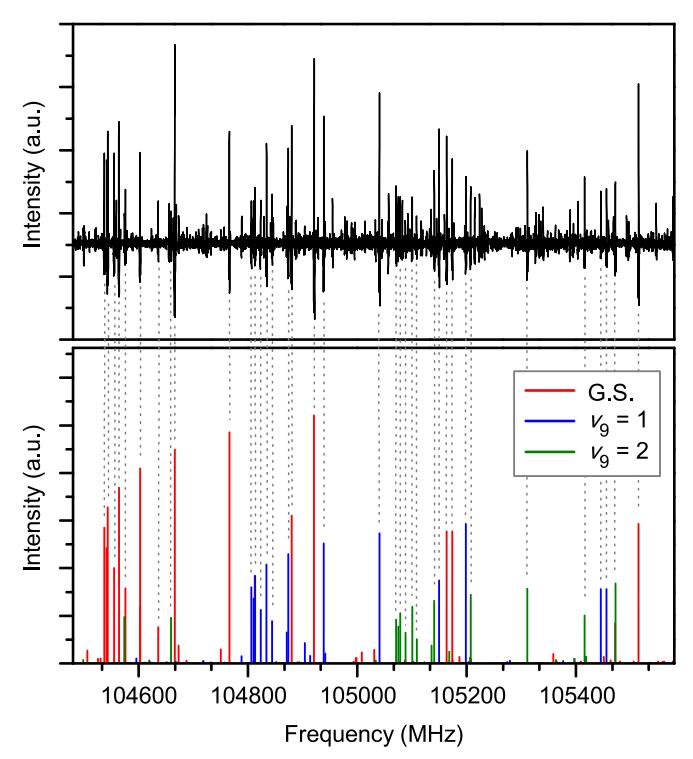


Figure 3. Section of the room-temperature millimeter-wave spectrum of HCCSCN. The upper panel shows the experimental spectrum, while the lower panel illustrates a stick reproduction of the ground state (G.S.) and $v_9 = 1$, 2 excited vibrational states using the spectroscopic constants from Table 1. The trend of the relative intensities is not always consistent in theory and experiment due to the performance of the experimental setup (multiplication chain, cell transmission, and detector sensitivity).

 $N_T \leqslant 5 \times 10^{15} \, \mathrm{cm}^{-2}$. This corresponds to a fractional abundance of $X_{\mathrm{H_2}} \leqslant 2 \times 10^{-9} \, \mathrm{cm}^{-2}$ assuming an $N_{\mathrm{H_2}} = 3 \times 10^{24} \, \mathrm{cm}^{-2}$ (A. Zernickel et al. 2012). We note that the $\mathrm{H_2}$ column density is derived from Herschel observations of the source and assume a homogeneous gas distribution over a 10'' emitting region toward the hot core. ALMA observations show this overall size is realistic but that the underlying gas distribution is heterogenous (S. J. El-Abd et al. 2024). As a result, this $\mathrm{H_2}$ column is a lower limit.

G+0.693-0.027. We also searched for the species toward the G+0.693-0.027 (hereafter G+0.693) molecular cloud located in the Sgr B2 complex in the Galactic center. This cloud is a well-suited target to address the search for HCCSCN because it exhibits an extremely rich chemical content (e.g., V. M. Rivilla et al. 2018, 2019, 2020, 2021a, 2021b, 2022a, 2022b, 2022c, 2023; S. Zeng et al. 2018, 2021, 2023;

Table 3
Rotational and Vibrational Partition Functions for HCCSCN at Different Temperatures

T(K)	$Q_{ m rot}$	$Q_{ m vib}$
1000.000	2063131.21	1851.5
500.000	724859.39	39.6
300.000	335584.98	6.3
225.000	217628.24	3.2
150.000	118273.41	1.7
75.000	41753.40	1.1
37.500	14755.85	1.0
18.750	5219.50	1.0
9.375	1848.40	1.0
5.000	722.22	1.0
3.000	337.21	1.0

L. F. Rodríguez-Almeida et al. 2021b; L. Colzi et al. 2022; I. Jiménez-Serra et al. 2022; S. Massalkhi et al. 2023; M. Sanz-Novo et al. 2023; D. San Andrés et al. 2024). In the last 5 years, 18 new interstellar molecules have been identified and among them several with sulfur, such as thioformic acid (HCOSH; L. F. Rodríguez-Almeida et al. 2021a), the O-protonated carbonyl sulfide (HOCS⁺; M. Sanz-Novo et al. 2024a), and thionylimide (HNSO; M. Sanz-Novo et al. 2024b). Moreover, it has been found that the relative abundances of S-bearing species with O-analogs are significantly higher than in other molecular clouds, suggesting that S is much less depleted in G+0.693, likely due to the action of large-scale shocks (M. Sanz-Novo et al. 2024a).

We performed the search of HCCSCN using a high-sensitivity spectral survey carried out with the Yebes 40 m and IRAM 30 m telescopes. The observations were carried out during sessions between 2021 March and 2022 March, with a total telescope scheduled time of 230 hr, of which 110 hr were on source. We used the position switching mode, centering the observations at $\alpha=17^{\rm h}47^{\rm m}22^{\rm s}$, $\delta=-28^{\circ}21'27''$, with the off position shifted by $\Delta\alpha=-885''$ and $\Delta\delta=290''$. The noise at this spectral resolution is $0.25-0.9\,\rm mK$, depending on the spectral range. The line intensity of the spectra was measured in units of T_A^* , since the molecular emission toward G+0.693 is extended over the beams (e.g., S. Brünken et al. 2010). More details of these observations were provided on V. M. Rivilla et al. (2023).

We implemented the spectroscopic entry of HCCSCN presented in this work into the MADCUBA package; 10

^a Calculated at the B3PLYP/6-311++G(d,p) level.

¹⁰ Madrid Data Cube Analysis on ImageJ is a software developed at the Center of Astrobiology in Madrid; http://cab.inta-csic.es/madcuba/.

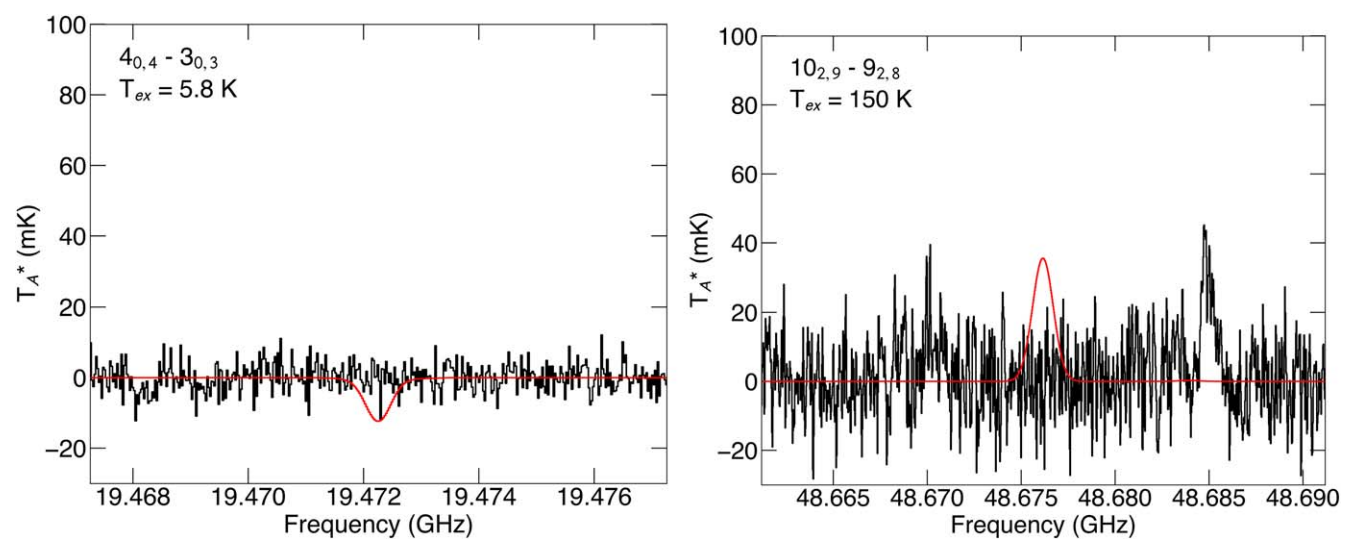


Figure 4. Transitions used to constrain the 3σ upper limit for HCCSCN in the GBT PRIMOS observations of Sgr B2(N) in the case of a cold, extended component in absorption (left) and a warm, compact component (right). Hyperfine splitting is not resolved at these line widths (see text), so the unresolved quantum numbers are provided.

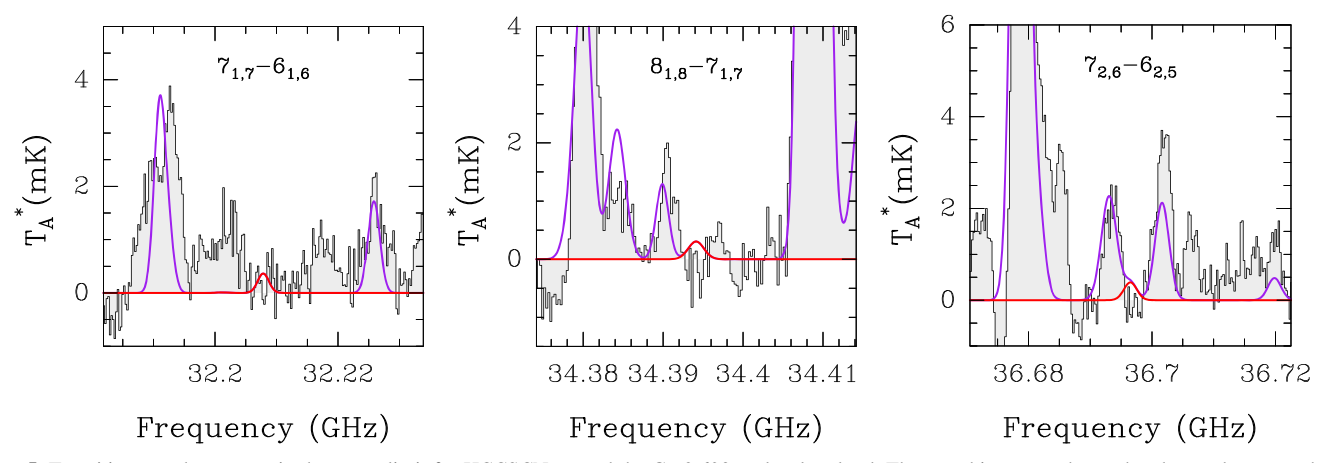


Figure 5. Transitions used to constrain the upper limit for HCCSCN toward the G+0.693 molecular cloud. The gray histogram shows the observed spectra, the red curve indicates the LTE model using the upper limit derived for the column density (see the text), and the purple line shows the line emission from all the molecules identified in the region (including the contribution of HCCSCN). As in Figure 4 hyperfine splitting is not resolved, so the unresolved quantum numbers are provided.

version 04/07/2023 (S. Martín et al. 2019). Using the Spectral Line Identification and Modeling (SLIM) tool of MADCUBA, we generated a synthetic spectra under the assumption of local thermodynamic equilibrium (LTE) and compared with the observed spectra. The species is not identified in the survey. Figure 5 shows the three brightest transitions according to the LTE model that are not blended with line emission of other molecules. We have thus derived with SLIM a 3σ upper limit (in integrated intensity), using typical parameters derived for other species in this cloud (line width of $20 \, \mathrm{km \, s^{-1}}$, excitation temperature of 8 K, and velocity of $68 \, \mathrm{km \, s^{-1}}$). We obtained a value of $N < 1.1 \times 10^{12} \, \mathrm{cm^{-2}}$. This translates into a fractional abundance with respect to H_2 of $< 8.1 \times 10^{-12}$, using $N(H_2) = 1.35 \times 10^{23} \, \mathrm{cm^{-2}}$ from S. Martin et al. (2008).

TMC-1. The observations of TMC-1 are part of the QUIJOTE¹¹ line survey (J. Cernicharo et al. 2021a, 2024). The data were gathered with the Yebes 40 m radio telescope equipped with the Q-band receivers and spectrometers built

under the Nanocosmos project.¹² The selected position corresponds to the cyanopolyyne peak in TMC-1 $(\alpha_{\rm J2000}=4^{\rm h}41^{\rm m}41^{\rm s}9$ and $\delta_{\rm J2000}=+25^{\circ}41'27.''0)$. The receivers consist of two cold high-electron mobility transistor amplifiers covering the 31.0–50.3 GHz band with horizontal and vertical polarizations. The receiver temperatures are 16 K at 32 GHz and 30 K at 50 GHz. The backends are $2\times8\times2.5$ GHz fast Fourier transform spectrometers with a spectral resolution of 38 kHz, providing the whole coverage of the Q-band in both polarizations. A more detailed description of the system is given by F. Tercero et al. (2021).

The data of the QUIJOTE line survey presented here were gathered in several observing runs between 2019 November and 2023 July. All observations are performed using frequency-switching observing mode with a frequency throw of 8 and 10 MHz. The total observing time on the source is 737 (frequency throw of 8 MHz) and 465 hr (frequency throw of 10 MHz). Hence, the total observing time on source is 1202 hr. The measured sensitivity varies between 0.08 mK at 32 GHz

¹¹ Q-band Ultrasensitive Inspection Journey to the Obscure TMC-1 Environment.

https://nanocosmos.iff.csic.es/

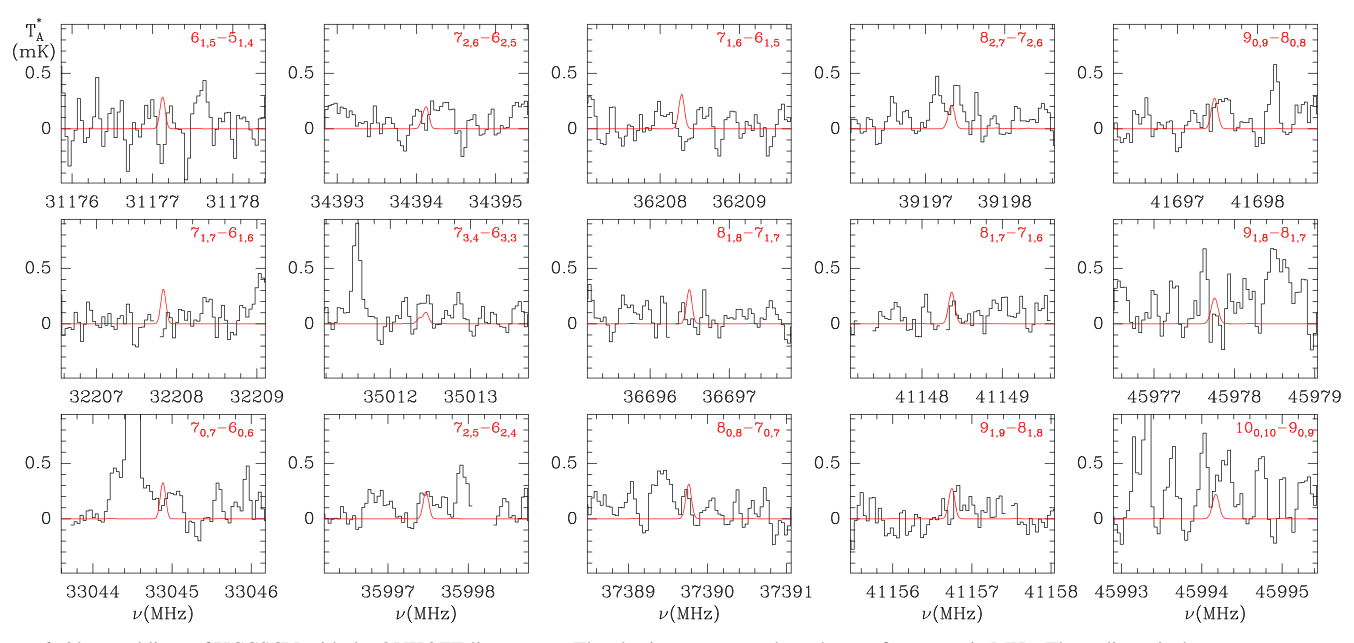


Figure 6. Observed lines of HCCSCN with the QUIJOTE line survey. The abscissa corresponds to the rest frequency in MHz. The ordinate is the antenna temperature corrected for atmospheric and telescope losses in mK. Blanked channels correspond to negative features produced in the folding of the frequency-switching data. The synthetic spectrum for each transition is shown in red. The physical parameters used to generate them are given in the text.

and 0.2 mK at 49.5 GHz. The data analysis procedure has been described by J. Cernicharo et al. (2022).

As a consequence of the unprecedented sensitivity of the QUIJOTE line survey, more than 50 new molecular species have been found in the last 4 years in TMC-1, including protonated species of abundant species, pure hydrocarbons, and radicals (see, e.g., J. Cernicharo et al. 2024, and references therein). Among these new molecules it is worth noting the detection of the S-bearing species NCS, HCCS, H2CCS, H2CCCS, C4S, HCSCN, HCSCCH, HC₄S, HCCCS⁺, HCCS, HCCS⁺, HSO, HCNS, and NCCHCS (J. Cernicharo et al. 2021b, 2021c, 2024; C. Cabezas et al. 2022, 2024; R. Fuentetaja et al. 2022; N. Marcelino et al. 2023). The presence of a large reservoir of S-bearing species in TMC-1, in particular of HCSCN, HCSCCH, NCCHCS, HCNS, HCSN, and HSCN (J. Cernicharo et al. 2021c, 2024; C. Cabezas et al. 2024), indicates that HCCSCN deserves to be searched in this source as it could be the CCH derivative of HSCN. The latter molecule has been found to be a factor of \sim 3 more abundant than HNCS with a column density of $8.3 \times 10^{11} \, \text{cm}^{-2}$ (J. Cernicharo et al. 2024).

The spectroscopic information of HCCSCN derived in this work has been implemented in the MADEX¹³ code. Because of the much larger value of the *a*-component of the dipole moment, only *a*-type transitions have been searched for. As the kinetic temperature of the cloud is 9 K (M. Agúndez et al. 2023), we limited the energy of the upper levels of the transitions to 14 K (J = 10, $K_a = 0,1$). In order to model the expected intensity we have assumed a source of uniform brightness temperature with a diameter of 80" (D. Fossé et al. 2001; J. Cernicharo et al. 2023). The adopted line width is 0.6 km s⁻¹, i.e., identical to that derived for similar species such as the CCH and CN derivative of thioformaldeyde, HCSCCH and HCSCN (J. Cernicharo et al. 2021c), and the CN derivative of thioketene, NCCHCS (C. Cabezas et al. 2024). We also adopted a rotational temperature of 5 K similar to that

5. Astrochemical Implications

Sulfur molecules, in general, are of great astrochemical interest, in part, because of the long-standing mystery of "missing sulfur," based on the apparent drop in observable sulfur species when comparing diffuse environments—where the abundances are roughly the solar values—to dense molecular clouds—where the combined abundances of all sulfur-bearing species can be 3 orders of magnitude less. It seems fairly clear that the sulfur is not disappearing, per se, but rather is being chemically converted to some reservoir species, which has not yet been conclusively identified. Sulfur is also an important element for terrestrial organisms, being a key constituent of biomolecules such as the amino acids cysteine and methionine, and thus, a better understanding of interstellar sulfur chemistry is an important step in understanding the inventory of prebiotic molecules that may be available for delivery to the surfaces of exoplanets and implicated in the origins of life.

In astrophysical environments, the synthesis pathways used to produce HCCSCN for this study would not occur. Indeed, unsaturated species such as HCCSCN are typical of the kinds of molecules formed via gas-phase reactions, which are almost exclusively barrierless, exothermic, two-body processes given the low temperatures ($\sim 10~\rm K$) and densities ($\sim 10^4~\rm cm^{-3}$) of molecular clouds. To the best of our knowledge, the only such reaction leading to HCCSCN that has been the subject of laboratory investigations is

$$HCCH + SCN \rightarrow HCCSCN + H,$$
 (1)

though, as reported by H.-T. Chen & J.-J. Ho (2003), this is an endothermic process with a substantial barrier, which is

derived for HCSCN. A total of 15 individual transitions were searched, as shown in Figure 6. Only a few of the generated synthetic spectra have a counterpart in the data, and hence, we conclude that the molecule is not present in TMC-1 with a 3σ upper limit to its column density, based on each individual line, of 5×10^{10} cm⁻².

¹³ https://nanocosmos.iff.csic.es/?page_id=1619

consistent with the upper limit of 10^{-14} cm³ s⁻¹ experimentally determined for the rate coefficient by R. E. Baren & J. F. Hershberger (1999) in the temperature range 298-620 K. Therefore, this is not a viable formation pathway in cold astrophysical environments. Nevertheless, recent observations of other sulfur-bearing species in TMC-1 (J. Cernicharo et al. 2021b, 2021c, 2024) yield some clues that could point to other possible formation pathways to HCCSCN. One possibility is the reactions of CN with H₂CCS and HCCSH. The first one is calculated to be endothermic by 10.3 kcal mol⁻¹, although the second is exothermic and could provide a valid route. Another possibility is the reactions of HCCS with HCN and HNC, although in this case the two are calculated to be endothermic by 44.1 and 29.2 kcal mol⁻¹, respectively. The exploration of the potential energy surface for the different reactions was done using the Molpro 2020.2 ab initio program package (H.-J. Werner & P. J. Knowles et al. 2020). All the stationary points were fully optimized using the coupled-cluster method (CCSD (T); K. Raghavachari et al. 1989) along with Dunning's correlation consistent polarized valence triple-z (cc-pVTZ) basis set (T. H. Dunning 1989), and the energies are relative to that of the separated reactants. The reaction $C_2S + H_2CN$ is calculated to be exothermic, although it is likely that it occurs with a barrier because there is an important rearrangement. Finally, the reaction C₂H + HSCN could be a source of HCCSCN at low temperatures because it is calculated to be exothermic and could occur with a minimal rearrangement.

However formed, gas-phase HCCSCN could be depleted via, e.g., photodissociation, reactions with other gas-phase species, or accretion onto grains. Once accreted onto the surfaces of dust grains or dust-grain ice mantles, the dominant chemical destruction pathway is via reaction with hydrogen atoms, which can remain comparatively mobile even at the very low temperature of 10 K. Previous quantum chemical calculations of the reaction of highly unsaturated interstellar molecules with H have found that such processes are often barrierless and exothermic and yield one or more stable, more highly saturated end products (C. N. Shingledecker et al. 2019, 2022). If formed on the surfaces of grains in cold molecular clouds, these stable, more highly saturated products can become covered by the continuous accretion of yet more gas-phase species, thereby becoming trapped within the dustgrain ice mantle. If the astrophysical environment subsequently warms, such as happens during star formation, these trapped molecules can be liberated into the gas phase, where they can be observed. Thus, it is often possible to surmise a chemical link between an unsaturated carbon chain molecule seen in a cold core with a more saturated species seen in a hot core. In the absence of detailed quantum calculations, it is not possible to say with a high degree of certainty what the grain-surface saturation of HCCSCN would yield, but we here suggest two possibilities by way of speculation. The first possibility is the species C₃H₅NS, i.e., the ethyl ester of thiocyanic acid. Another, more astrochemically interesting possible saturation product is C₃H₃NS, the heterocyclic molecule thiazole. This latter species would be of particular interest since, though now several cyclic or polycyclic species have been detected in the ISM, there are to date no detections of heterocycles with a sulfur atom and certainly not of cycles with two heteroatoms

such as thiazole, and if it were detected, it would suggest a grain-surface origin for other similar species.

6. Conclusions

We have determined for the first time precise rotational and centrifugal distortion constants for the CCH derivative of HSCN (HCCSCN) from accurate laboratory measurements. This new laboratory data allowed us to search for it toward several interstellar sources without success. Several possible formation paths of this species are discussed, emphasizing that it could be formed from the reaction of CCH with HSCN. Similar reactions have been previously proposed for other S-bearing species found in TMC-1 such as HCSCN, HCSCCH, and NCCHCS, which are CN and CCH derivatives of H₂CS and H₂CCS that are very abundant in that cloud. Although no spectral features of HCCSCN were found, present data can be used with confidence in future searches in other interstellar sources.

Acknowledgments

The National Radio Astronomy Observatory is a facility of the National Science Foundation operated under cooperative agreement by Associated Universities, Inc. This paper makes use of the following ALMA data: ADS/JAO.ALMA#2015. A.00022.T. ALMA is a partnership of ESO (representing its member states), NSF (USA), and NINS (Japan), together with NRC (Canada), MOST and ASIAA (Taiwan), and KASI (Republic of Korea), in cooperation with the Republic of Chile. The Joint ALMA Observatory is operated by ESO, AUI/ NRAO, and NAOJ. E.R.A. and I.L. acknowledge funding from Ministerio de Ciencia e Innovación (PID2019-111396GB-I00) and Junta de Castilla y León (VA244P20). V.M.R., I.J.-S., and J.M.-P. acknowledge support from grant No. PID2022-136814NB-I00 by the Spanish Ministry of Science, Innovation and Universities/State Agency of Research MICIU/AEI/ 10.13039/501100011033 and by ERDF, UE. V.M.R. also acknowledges support from the grant No. RYC2020-029387-I funded by MICIU/AEI/10.13039/501100011033 and by "ESF, Investing in your future" and from the Consejo Superior de Investigaciones Científicas (CSIC) and the Centro de Astrobiología (CAB) through project 20225AT015 (Proyectos intramurales especiales del CSIC). J.C., C.C., and M.A. thank the Spanish Ministry of Science, Innovation and Universities for funding support through projects PID2019-106110GB-I00 and PID2019-106235GB-I00 and ERC for funding through grant ERC-2013-Syg-610256-NANOCOSMOS. M.A. thanks the Consejo Superior de Investigaciones Científicas (CSIC; Spain) for funding through project PIE 202250I097. J.-C.G. thanks the Programme National "Physique et Chimie du Milieu Interstellaire" (PCMI) of CNRS Terre @ Univers with CNRS Physique & CNRS Chimie, cofunded by CEA and CNES.

ORCID iDs

Elena R. Alonso https://orcid.org/0000-0001-5816-4102
Aran Insausti https://orcid.org/0000-0002-9291-1762
Lucie Kolesniková https://orcid.org/0000-0003-3567-0349
Iker León https://orcid.org/0000-0002-1992-935X
Brett A. McGuire https://orcid.org/0000-0003-1254-4817
Christopher N. Shingledecker https://orcid.org/0000-0002-5171-7568

Marcelino Agúndez https://orcid.org/0000-0003-3248-3564

```
José Cernicharo https://orcid.org/0000-0002-3518-2524
Víctor M. Rivilla https://orcid.org/0000-0002-2887-5859
Carlos Cabezas https://orcid.org/0000-0002-1254-7738
Izaskun Jiménez-Serra https://orcid.org/0000-0003-4493-8714
Jesús Martín-Pintado https://orcid.org/0000-0003-4561-3508
Jean-Claude Guillemin https://orcid.org/0000-0002-2929-057X
```

References

```
Adande, G. R., Halfen, D. T., Ziurys, L. M., Quan, D., & Herbst, E. 2010, ApJ,
Agúndez, M., Marcelino, N., Cernicharo, J., & Tafalla, M. 2018, A&A,
   611, L1
Agúndez, M., Marcelino, N., Tercero, B., & Cernicharo, J. 2023, A&A,
   677. L13
Baren, R. E., & Hershberger, J. F. 1999, JPCA, 103, 11340
Becke, A. D. 1992, JChPh, 96, 2155
Becke, A. D. 1993, JChPh, 98, 1372
Belloche, A., Muller, H. S. P., Menten, K. M., Schilke, P., & Comito, C. 2013,
   A&A, 559, A47
Brünken, S., Belloche, A., Martin, S., Verheyen, L., & Menten, K. M. 2010,
      A. 516, A109
Brünken, S., Yu, Z., Gottlieb, C. A., McCarthy, M. C., & Thaddeus, P. 2009,
   ApJ, 706, 1588
Cabezas, C., Agundez, M., Endo, Y., et al. 2024, A&A, 686, L3
Cabezas, C., Agúndez, M., Marcelino, N., et al. 2022, A&A, 657, L4
Cabezas, C., Varela, M., & Alonso, J. L. 2017, Angew. Chem. Int., 56, 6420 Cernicharo, J., Agúndez, M., Cabezas, C., et al. 2024, A&A, 682, L4
Cernicharo, J., Agúndez, M., Kaiser, R. I., et al. 2021a, A&A, 652, L9
Cernicharo, J., Cabezas, C., Agúndez, M., et al. 2021b, A&A, 648, L3
Cernicharo, J., Cabezas, C., Endo, Y., et al. 2021c, A&A, 650, L14
Cernicharo, J., Cabezas, C., Endo, Y., et al. 2021d, A&A, 646, L3
Cernicharo, J., Fuentetaja, R., Cabezas, C., et al. 2022, A&A, 663, L5
Cernicharo, J., Lefloch, B., Agúndez, M., et al. 2018, ApJL, 853, L22
Cernicharo, J., Tercero, B., Marcelino, N., Agúndez, M., & de Vicente, P.
   2023, A&A, 674, L4
Chen, H.-T., & Ho, J.-J. 2003, JPCA, 107, 7004
Colzi, L., Martín-Pintado, J., Rivilla, V. M., et al. 2022, ApJL, 926, L22
Daly, A. M., Kolesnikova, L., Mata, S., & Alonso, J. L. 2014, JMoSp, 306, 11
Dunning, T. H., Jr. 1989, JChPh, 90, 1007
El-Abd, S. J., Brogan, C. L., Hunter, T. R., et al. 2024, APJ, 1
Endres, C. P., Schlemmer, S., Schilke, P., Stutzki, J., & Muller, H. S. P. 2016,
   JMoSp, 327, 95
Foley, H. M. 1947, PhRv, 71, 747
Fossé, D., Cernicharo, J., Gerin, M., & Cox, P. 2001, ApJ, 552, 168
Frerking, M. A., Linke, R. A., & Thaddeus, P. 1979, ApJL, 234, L143
Frisch, M. J., Pople, J. A., & Binkley, J. S. 1984, JChPh, 80, 3265
Frisch, M. J., Trucks, G. W., Schlegel, H. B., et al. 2016, Gaussian 16
   Revision B.01
Fuente, A., Goicoechea, J. R., Pety, J., et al. 2017, ApJL, 851, L49
Fuentetaja, R., Agúndez, M., Cabezas, C., et al. 2022, A&A, 667, L4
Gordy, W., & Cook, R. L. 1984, Microwave Molecular Spectra (New York:
   Wiley-Interscience)
Grimme, S., Antony, J., Ehrlich, S., & Krieg, H. 2010, JChPh, 132, 154104
Grimme, S., Ehrlich, S., & Goerigk, L. 2011, JCoCh, 32, 1456
Halfen, D. T., Ziurys, L. M., Brünken, S., et al. 2009, ApJL, 702, L124
Jiménez-Serra, I., Rodríguez-Almeida, L. F., Martín-Pintado, J., et al. 2022,
    A&A, 663, A181
Kolesniková, L., Alonso, E. R., Mata, S., & Alonso, J. L. 2017, ApJS, 229, 26
```

```
León, I., Alonso, E. R., Cabezas, C., Mata, S., & Alonso, J. L. 2019, CmChe,
  2. 3
Lis, D. C., & Goldsmith, P. F. 1990, ApJ, 356, 195
Lu, B., Wu, Z., Wang, L., et al. 2021, ChCom, 57, 3343
Marcelino, N., Puzzarini, C., Agúndez, M., et al. 2023, A&A, 674, L13
Martín, S., Martín-Pintado, J., Blanco-Sánchez, C., et al. 2019, A&A,
  631, A159
Martin, S., Requena-Torres, M. A., Martin-Pintado, J., & Mauersberger, R.
  2008, ApJ, 678, 245
Massalkhi, S., Jiménez-Serra, I., Martín-Pintado, J., et al. 2023, A&A,
  678, A45
McGuire, B. A., Carroll, P. B., Loomis, R. A., et al. 2016, Sci, 352, 1449
McGuire, B. A., Martin-Drumel, M.-A., Thorwirth, S., et al. 2016, PCCP, 18,
McGuire, B. A., Shingledecker, C. N., Willis, E. R., et al. 2017, ApJL,
   851, L46
Møller, C., & Plesset, M. S. 1934, PhRv, 46, 618
Neill, J. L., Muckle, M. T., Zaleski, D. P., et al. 2012, ApJ, 755, 153
Pickett, H. M. 1991, JMoSp, 148, 371
Pickett, H. M., Poynter, R. L., Cohen, E. A., et al. 1998, JQSRT, 60, 883
Raghavachari, K., Trucks, G. W., Pople, J. A., & Head-Gordon, M. 1989, CPL,
  157, 479
Reid, M. J., Menten, K. M., Brunthaler, A., et al. 2014, ApJ, 783, 130
Rivilla, V. M., Colzi, L., Jiménez-Serra, I., et al. 2022a, ApJL, 929, L11
Rivilla, V. M., García De La Concepción, J., Jiménez-Serra, I., et al. 2022b,
  FrASS, 9, 829288
Rivilla, V. M., Jiménez-Serra, I., García de la Concepción, J., et al. 2021a,
   MNRAS, 506, L79
Rivilla, V. M., Jiménez-Serra, I., Martín-Pintado, J., et al. 2021b, PNAS, 118,
  2101314118
Rivilla, V. M., Jiménez-Serra, I., Martín-Pintado, J., et al. 2022c, FrASS, 9,
Rivilla, V. M., Martín-Pintado, J., Jiménez-Serra, I., et al. 2018, MNRAS,
  483, L114
Rivilla, V. M., Martin-Pintado, J., Jimenez-Serra, I., et al. 2019, MNRAS,
  483, L114
Rivilla, V. M., Martín-Pintado, J., Jiménez-Serra, I., et al. 2020, ApJL,
  899, L28
Rivilla, V. M., Sanz-Novo, M., Jiménez-Serra, I., et al. 2023, ApJL, 953, L20
Robinson, G. W., & Cornwell, C. D. 1953, JChPh, 21, 1436
Rodríguez-Almeida, L. F., Jiménez-Serra, I., Rivilla, V. M., et al. 2021a, ApJL,
  912, L11
Rodríguez-Almeida, L. F., Rivilla, V. M., Jiménez-Serra, I., et al. 2021b, A&A,
  654, L1
San Andrés, D., Rivilla, V. M., Colzi, L., et al. 2024, ApJ, 967, 39
Sanz-Novo, M., Rivilla, V. M., Jiménez-Serra, I., et al. 2023, ApJ, 954, 3
Sanz-Novo, M., Rivilla, V. M., Jiménez-Serra, I., et al. 2024a, ApJ,
Sanz-Novo, M., Rivilla, V. M., Müller, H. S. P., et al. 2024b, ApJL, 965, L26
Shingledecker, C. N., Alvarez-Barcia, S., Korn, V. H., & Kastner, J. 2019, ApJ,
Shingledecker, C. N., Banu, T., Kang, Y., et al. 2022, JPCA, 126, 5343
Tercero, F., López-Pérez, J. A., Gallego, J. D., et al. 2021, A&A, 645, A37
Turner, B. E. 1991, ApJS, 76, 617
Vidal, T. H. G., Loison, J.-C., Jaziri, A. Y., et al. 2017, MNRAS, 469, 435
Watson, J. K. G. 1977, in Vibrational Spectra and Structure, Vol. 6 ed.
  J. R. Durig (Amsterdam: Elsevier), 1
Werner, H.-J., Knowles, P. J., et al. 2020, MOLPRO, 2020.2, A Package of
  ab initio Programs, https://www.molpro.net
Wierzejewska, M., & Moc, J. 2003, JPCA, 107, 11209
Zeng, S., Jimenez-Serra, I., Rivilla, V. M., et al. 2018, MNRAS, 478, 2962
Zeng, S., Jiménez-Serra, I., Rivilla, V. M., et al. 2021, ApJL, 920, L27
Zeng, S., Rivilla, V. M., Jiménez-Serra, I., et al. 2023, MNRAS, 523, 1448
Zernickel, A., Schilke, P., Schmiedeke, A., et al. 2012, A&A, 546, A87
```